

## Review Paper:

**Determination of seismic wave attenuation: A Review**

Banerjee Soham and Kumar Abhishek\*

Department of Civil Engineering, Indian Institute of Technology Guwahati, Amingaon Guwahati Assam 781039, INDIA

\*abhiak@iitg.ernet.in

**Abstract**

Earthquake occurs when pent up energy is released during tectonic activities. This energy spreads in the form of waves and while propagating, these waves attenuate non-uniformly in different directions due to the variation in the elastic properties of the propagation medium. The recorded amplitudes of seismic waves are directly related to the attenuation properties of the medium. Compressional wave ( $P$  wave) and shear wave ( $S$  wave) are the primary waves (also known as direct waves) generated during an earthquake (EQ) and do significant damages within a certain range (200 km).

Hence, attenuation studies for these waves are pretty much important in seismic hazard estimation. Various approaches had been developed worldwide to study the attenuation of these waves. In one of the approach, coda wave (backscattered waves generated when direct waves interact with the medium heterogeneities) amplitudes are used to normalize the direct wave amplitudes in order to determine the frequency dependent attenuation of direct waves. Obtained attenuation values can be used to understand the tectonic stability and medium heterogeneities of a region.

Further, using these values intrinsic and scattering attenuations can be obtained separately in a region. In this study, a delineate discussion reviewing the properties of coda wave and coda normalization method (CNM) is given. In addition to CNM, two more methods in order to determine the attenuation of direct waves are also presented here. A detailed comparison in terms of assumptions made while developing each of the above methods is carried out here. Further, a detailed summary of various studies, addressing the attenuation characteristics of direct waves based on the above three methods is presented here. Regional characteristics such as medium heterogeneity, tectonic stability etc. evaluated by various researchers based on the direct wave attenuation are also discussed in this paper.

**Keywords:** Direct wave attenuation, intrinsic attenuation, scattering attenuation, medium heterogeneity, Coda normalization method.

**Introduction**

When a mechanical wave propagates through a medium, a gradual decay of wave amplitude can be observed before the wave diminishes. This phenomenon is called the attenuation of seismic waves and is an important characteristic in the modern seismology which needs to be studied. The presence of faults, folds, dykes, sills etc. changes the elastic properties of the medium resulting in heterogeneous medium. The scale of heterogeneity varies from region to region. According to the scale of heterogeneity, the waves may attenuate differently in different regions. This variation in attenuation also contributes to the variation in spectral amplitude of waves along with the site amplification, resulting in a variation in the reported damages even among sites with similar hypocentral distances ( $r$ ).

Hence, attenuation study is important to understand which part of the region will be more affected due to lesser attenuation of wave in case of earthquake (EQ) occurrence in the nearby region. The attenuation study is also important for ground motion prediction<sup>5</sup> and seismic hazard analysis. The attenuation of wave is defined by the inverse of quality factor ( $Q^{-1}$ ) while quality factor ( $Q$ ) is the wave transmission quality of the medium. Knopoff<sup>13</sup> defined the attenuation of wave in terms of energy as<sup>12</sup>:

$$Q^{-1} = -\frac{\Delta E}{2\pi E}$$

where  $\Delta E$  is the loss of energy per cycle and  $E$  is the total energy of the wave. The attenuation of seismic waves occurs due to geometrical spreading, scattering of seismic energy and inelasticity of the propagation medium<sup>19</sup>.

Geometrical spreading defines the attenuation of the seismic energy due to the distribution of wave energy over the surface of the spherical wavefront. When a mechanical energy ( $E_0$ ) starts propagating from its source, it spreads in a spherical wavefront such that at radial distance ' $r$ ' from the point of origin, the energy at the wavefront would be<sup>12</sup>:

$$E(r) = \frac{E_0}{4\pi r^2}$$

Thus, with an increase in the wavefront radius ( $r$ ), surface area ( $4\pi r^2$ ) of the spherical wavefront also increases. As a result, there is a decrease in the intensity of wave energy  $E(r)$  at any particular point on the surface of that spherical wavefront. Furthermore, seismic energy is proportional to the square of the wave amplitude ( $A$ ) i.e.  $E(r) \propto A^2$ . Collectively, based on the above two observations, it can be concluded that amplitude of seismic wave ( $A$ ) is inversely proportional to the hypocentral distance<sup>12</sup> ( $r$ ) i.e.

$$A^2 \alpha \frac{1}{r^2} \rightarrow A \alpha \frac{1}{r}$$

Scattering attenuation on the other hand occurs due to the presence of heterogeneities in the wave propagation medium. As the seismic wave passes through a medium, it interacts with the medium heterogeneities and the wave energy gets redistributed causing attenuation due to multiple reflections within that medium. On the other hand, intrinsic attenuation occurs due to inelasticity of the medium. As a result of which, a portion of energy the wave carries is transformed into heat<sup>14</sup>. Thus, the energy generated at the EQ source attenuates mainly in three possible forms as discussed above. Detailed assessment of attenuation characteristics of a medium if attempted, will help in understanding the medium characteristics such as heterogeneity, inelasticity etc. between the EQ source and the target site. Numerous researchers attempted to understand the attenuation characteristics of medium, correlating the same with each of the above medium properties.

During an EQ recording, ground motion record shows first the arrival of P wave followed by S wave, surface wave and at last coda wave. Aki<sup>2</sup> first time introduced the existence of coda wave on a seismogram. Later, Aki and Chouet<sup>4</sup> presented a detailed discussion about the origin and properties of coda wave. As per Aki and Chouet<sup>4</sup>, three possible reasons about the origins of coda wave were thought of namely; slow surface wave, aftershock wave and backscattered wave. Surface wave is a combination of direct wave and aftershock wave which is also a direct wave in itself. It has been found from studies<sup>1</sup> that direct wave amplitude mitigates as  $r$  increases whereas coda wave amplitude seems indifferent with the changes in  $r$ . For this reason, the first two thoughts (slow surface and aftershock waves) about the origin of coda wave were discarded.

However, the third possible thought (backscattered wave) complied with the coda wave properties. This observation was confirmed by Aki and Chouet<sup>4</sup> from the array analysis data based on the mining blast performed by Scheimer and Landers<sup>22</sup>. Peak energy within a frequency ( $f$ ) range of 1-2Hz was recorded for S and coda wave. From the array analysis, Aki and Chouet<sup>4</sup> found that S wave signals showed arrival of maximum energy from the blast direction whereas in case of coda waves, maximum energy was arriving from almost all the directions. Thus, Aki and Chouet<sup>4</sup> concluded that the coda waves arrive at a seismic station from all the direction and not from the direction of EQ source alone.

This confirmed that coda waves are not direct waves coming from the EQ source but are backscattered waves generated due to the presence of medium heterogeneities. Further, Aki and Chouet<sup>4</sup> proposed two mathematical models in order to validate the origin of coda wave. First model was a single scattering model in which the total

energy of coda wave was considered as the summation of energy carried by each of the backscattered wavelets, originated from a single source and without the presence of other scatterers. In this model, scattering was considered as a weak process following the born approximation<sup>4</sup>, suggesting no energy loss in direct wave due to medium inelasticity or due to multiple scattering. Thus, the laws of conservation of energy were violated in the first model. The second model on the contrary was based on energy conservation and where the seismic energy was scattered through the diffusion process<sup>4</sup>.

Later, Aki<sup>3</sup> considered coda wave as backscattered wave and developed CNM in order to study the attenuation of direct S wave ( $Q_S^{-1}$ ). CNM proposed by Aki<sup>3</sup> was based on the properties of coda wave which arrives at the tail end of the seismogram. Later, Yoshimoto et al<sup>30</sup> extended CNM to study the attenuation of direct P wave ( $Q_P^{-1}$ ). It has to be highlighted here that direct P or S waves resemble P or S waves travelled directly from the source and recorded at the site without reflecting or refracting within the propagation medium. Detailed discussion about various properties of coda wave and the development of CNM are presented in this paper. Further, the determination of direct wave (P and S) attenuation in a medium, attempted by various researchers, using CNM is also presented here.

### Properties of Coda wave

In order to explore the coda wave properties, Aki<sup>2</sup> considered ground motion records from two aftershocks during 1966. These ground motions were recorded at two stations such that one station was nearer to first aftershock source while the other station was nearer to the second aftershock source. Juxtaposing these ground motion records, Aki<sup>2</sup> found that the tail end of all the seismograms which resembles the arrival of coda wave at the station looks similar and independent of  $r$ . However, the portion of ground motion records resembling direct waves (P and S) keeps on decreasing. To illustrate the above findings by Aki<sup>2</sup>, ground motion recorded during 2008 Pithoragarh EQ (M=4.3) is considered in the present work.

Recorded ground motions at four stations (Munsiyari, Kapkot, Pithoragarh and Champawat) are presented in figure 1 (a-d). Munsiyari being closest to the EQ source ( $r=22.11\text{km}$ ) shows a peak amplitude of  $13.44\text{cm/sec}^2$  as shown in figure 1(a). Similarly, for Kapkot ( $r=24.20\text{km}$ ), Pithoragarh ( $r=78.24\text{km}$ ) and Champawat ( $r=104.23\text{km}$ ), peak amplitudes of  $11.65\text{cm/sec}^2$ ,  $4.49\text{cm/sec}^2$  and  $3.16\text{cm/sec}^2$  respectively are observed as shown in Figure 1(b-d). Collectively, based on figure 1(a-d) it can be said that with the increase in  $r$ , the peak amplitude of the direct wave decreases.

On the other hand, in order to understand the effect of  $r$  at the tail end of the seismogram resembling the coda wave part, enlarged portion of the tail end corresponding to

figure 1(a-d) are shown in figure 2(a-d). Based on tail end presented in figure 2(a-d), it can be observed that for all four stations (Munsyari, Kapkot, Pithoragarh and Champawat) listed above, with the increase in  $r$ , peak amplitudes are found as  $0.2\text{cm/sec}^2$ ,  $0.3\text{cm/sec}^2$ ,  $0.6\text{cm/sec}^2$  and  $0.2\text{cm/sec}^2$  respectively.

In other words, no trend of significant variation in the coda amplitude  $A_c$  is seen with the change in the value of  $r$  as was observed in case of direct waves. Slight variation in  $A_c$  however may be due to the difference in the site amplification factor at all the above four stations. This effect of site amplification factor however was taken into account in the formulation of CNM. It has to be highlighted here that all the four stations considered above are in close proximity with respect to each other. As a result of which factors such as medium heterogeneities and source effect are similar for all the above recording stations.

Aki and Chouet<sup>4</sup> also pointed out that the value of  $A_c$  decays with the increasing lapse time ( $t_c$ ). To understand this observation, a MATLAB program is developed in the present work to find out the peaks within the coda window considering a sliding window length of 1s. The coda window is defined as the time interval between arrival of coda wave and the end of ground motion record on a seismogram. According to Yoshimoto et al<sup>30</sup>, the coda window should be considered at  $t_c \geq 2t_s$  ( $S$  wave arrival time) from the origin, in order to avoid the direct  $S$  wave data into the coda wave data. Ground motions recorded at above four stations [shown in figure 1(a-d)] are analyzed using the developed MATLAB code for determination of  $A_c$  at different  $t_c$ . Obtained  $A_c$  are then plotted with the corresponding values of  $t_c$  as shown in figure 3. It can be observed from figure 3 that the coda decay envelope represented by the linear pattern in figure 3 follows similar pattern for the above four recording stations. A decrease in the values of  $A_c$  with the increase in the value of  $t_c$  is observed as shown in figure 3 and is consistent with the observation by Aki and Chouet<sup>4</sup>.

Aki and Chouet<sup>4</sup> also found that  $A_c$  is independent of EQ magnitude for magnitude less than 6. To exemplify this observation, ground motions during four EQs with magnitude range from 3.9-5.1 recorded at Kapkot station between 2008 and 2010 are shown in figure 4(a-d). The peak amplitudes of the direct wave obtained from figure 4(a-d) are found as  $34.10\text{cm/s}^2$ ,  $23.45\text{cm/s}^2$ ,  $27.06\text{cm/s}^2$  and  $8.68\text{cm/s}^2$  for the ground motion records of EQs with magnitude 3.9, 4.3, 4.7 and 5.1 respectively.

Based on figure 4(a-d), a variation in the peak amplitude with respect to magnitude and  $r$  can be observed, however, no clear trend in the variation pattern can be found. On the

other hand, for seismograms presented in figure 4(a-d), the tail ends suggesting the coda part of all the ground motion records show a similar peak irrespective of EQ magnitude and  $r$ . In order to validate this observation further, the above developed MATLAB code is used to find out the peaks within the  $t_c$  considering a sliding window length of 1.5s each in all the four ground motion records. Obtained peaks from each of the four records are plotted against the corresponding values of  $t_c$  as shown in figure 5. It can be seen from figure 5 that the coda decay envelopes in this case are showing similar trend (decrease in  $A_c$  with increase in  $t_c$ ) for all the four seismograms.

Based on the observations made above, various properties of coda wave are enumerated below:

1. The value of  $A_c$  is independent of  $2r$ .
2. The coda decay envelope decreases with the increase in  $t_c$ .
3. The value of  $A_c$  is also independent of the EQ magnitude for magnitudes less than 6.

Along with the above properties of coda waves listed, some facts also exist as listed below:

- a) The total duration of the seismogram starting from the  $P$  wave onset time to the end of the coda wave (when signal to noise ratio becomes lesser than a certain threshold value) within  $r$  value of 100km is similar<sup>4</sup>. This is due to the fact that the direct waves are generated during the entire rupture time (fault rupture length divided by rupture velocity). Surface waves and coda waves are generated from these direct waves. The duration of surface waves and coda waves is thus dependent on rupture time. Hence, the total duration of seismogram remains same for all the recording stations within  $r$  value of 100km. However, beyond 100km though all the waves (direct, surface and coda) exist but the signal to noise ratio becomes significantly less resulting an apparent decrease in the total duration.
- b) The site amplification factor for coda wave was found same as that of direct  $S$  wave suggesting that coda wave is primarily composed of backscattered  $S$  wave.<sup>11, 28</sup>
- c) The velocity of coda wave ( $v_c$ ) was found matching with the velocity of direct  $S$  wave ( $v_s$ ) supporting the fact that coda wave is mainly comprised of  $S$  wave.<sup>11</sup>
- d) Based on the seismograms recorded at bedrock, Sato et al<sup>11</sup> confirmed that the coda wave originates due to medium heterogeneities and not due scattering from the surface.

### Coda Normalization Method (CNM)

Based on the properties of coda wave explained above, it can be seen that coda window of the seismogram is similar for ground motions recorded at different stations irrespective of  $r$  and EQ magnitude. Yoshimoto et al<sup>30</sup>

normalized direct wave part with respect to coda wave part of ground motion records and termed it as CNM to determine the attenuation of direct waves in a medium. Detailed derivation of the CNM as per Yoshimoto et al<sup>30</sup> is discussed below:

The spectral amplitude of coda wave  $A_c(f, t_c)$  at  $t_c$  for a particular  $f$  can be written as<sup>30</sup>:

$$A_c(f, t_c) = S_s(f)P(f, t_c)G(f)I(f) \tag{1}$$

where  $S_s(f)$  is the source spectral amplitude of direct S waves,  $P(f, t_c)$  is the coda excitation factor which represents the spectral amplitude decay of coda wave with increasing  $t_c$ ,  $G(f)$  is the site amplification factor and  $I(f)$  is the instrumental response for that ground motion. Clearly, equation 1 shows that  $A_c(f, t_c)$  is independent of  $r$  but varies with  $t_c$  and  $f$ .

In case of direct S wave, the spectral amplitude  $A_s(f, r)$  varies with  $r$  which can be written as<sup>30</sup>:

$$A_s(f, r) = R_{\theta\phi} S_s(f) r^{-\gamma} \exp\left(-\frac{\pi f}{Q_s(f) V_s} r\right) G(f, \phi) I(f) \tag{2}$$

where  $R_{\theta\phi}$  is the source radiation factor,  $\gamma$  is the geometrical spreading factor,  $Q_s(f)$  is the quality factor for S wave,  $V_s$  is the average S wave velocity within the range of  $r$ ,  $G(f, \phi)$  is the site amplification factor which depends on the incident angle of S wave ( $\phi$ ).

As the name suggests, CNM uses the value of  $A_s(f, r)$  normalized by  $A_c(f, t_c)$  (equation 2 divided by equation 1) as shown below<sup>30</sup>:

$$\frac{A_s(f, r)}{A_c(f, t_c)} = R_{\theta\phi} r^{-\gamma} \frac{G(f, \phi)}{G(f)} P^{-1}(f, t_c) \exp\left(-\frac{\pi f}{Q_s(f) V_s} r\right) \tag{3}$$

As per equation 1, for a fixed  $t_c$ , the value of  $P^{-1}(f, t_c)$  is only a function of  $f$  and can be written as  $Constant(f)$ . Thus, taking logarithm of equation 3 as per Yoshimoto et al<sup>30</sup> can be written as:

$$\ln\left(\frac{R_{\theta\phi}^{-1} A_s(f, r) r^\gamma}{A_c(f, t_c)}\right) = -\frac{\pi f}{Q_s(f) V_s} r + \ln\left(\frac{G(f, \phi)}{G(f)}\right) + Constant(f) \tag{4}$$

In order to determine the attenuation of direct S wave ( $Q_s^{-1}$ ), Yoshimoto et al<sup>30</sup> made assumptions regarding the source and site parameters. The effect of  $R_{\theta\phi}$  disappears

when large database of numerous EQs with varying  $r$  is considered for the analysis. Similarly, the ratio  $G(f, \phi)/G(f)$  becomes independent of  $\phi$  when many EQs are considered for the analysis. In such a case, the value of  $\phi$  is averaged for all the EQ records. Hence, the value of  $G(f, \phi)/G(f)$  also becomes a variable of  $f$  alone similar to  $P^{-1}(f, t_c)$ . This assumption was also supported by Tsujiura<sup>28</sup>. Thus, equation 4 can further be simplified as per Yoshimoto et al<sup>30</sup> below:

$$\ln\left(\frac{A_s(f, r) r^\gamma}{A_c(f, t_c)}\right) = -\frac{\pi f}{Q_s(f) V_s} r + Constant(f) \tag{5}$$

Above discussed method was extended for the determination of P wave attenuation ( $Q_p^{-1}$ ) by Yoshimoto et al<sup>30</sup>. Though the spectral shapes of P and S waves are different, it was assumed that for narrow ranges of  $f$  and EQs magnitude, the ratio of source spectral amplitude of P and S wave  $S_s(f)/S_p(f)$  becomes a function of  $f$  only as shown below<sup>30</sup>:

$$\frac{S_s(f)}{S_p(f)} = Constant(f) \tag{6}$$

Considering equation (1) and (6) above, Yoshimoto et al<sup>30</sup> concluded that  $A_c(f, t_c)$  is proportional to  $S_s(f)$  as well as  $S_p(f)$  as indicated by the following equation:

$$A_c(f, t_c) \propto S_s(f) \propto S_p(f) \tag{7}$$

Equation 7 above indicates that  $A_c(f, t_c)$  can also be expressed in terms of  $S_p(f)$ . To determine  $Q_p^{-1}$  by CNM, spectral amplitude of P wave  $A_p(f, r)$  is normalized by  $A_c(f, t_c)$  similar to the case of S wave shown in equation 3. A simplified form for P wave, similar to equation 5 can be obtained as shown below<sup>30</sup>:

$$\ln\left(\frac{A_p(f, r) r^\gamma}{A_c(f, t_c)}\right) = -\frac{\pi f}{Q_p(f) V_p} r + Constant(f) \tag{8}$$

It can be observed from the functional forms that equations 5 and 8 represent straight lines having slope of  $-\frac{\pi f}{Q(f) V}$  and constant ( $f$ ) as the intercept.

### Procedure for CNM based analysis

To determine the attenuation characteristics of a region, ground motions from numerous EQs recorded at seismic stations within that region are required. In CNM analysis, error in the obtained attenuation value decreases with the increase in number of EQ records used. On seismograms,

arrival time of direct P wave ( $t_p$ ) can be detected visually. The S wave arrival time ( $t_s$ ) can be determined either visually or by considering average velocities of P ( $v_p$ ) and S wave ( $v_s$ ) and using these following equations:

$$\Delta t_{ps} = r \left( \frac{1}{v_s} - \frac{1}{v_p} \right) \quad (9)$$

$$t_s = t_p + \Delta t_{ps} \quad (10)$$

For the analysis, direct wave data can be selected from the onset of direct waves (P or S) for a specific time window length<sup>30</sup>. As mentioned previously, coda wave data can be selected after  $t_c \geq 2t_s$ . Time window length used above for the case of direct waves should be used for coda wave too. The direct wave and coda wave data are then filtered using Butterworth Band-Pass filter for various ranges of  $f$ . In the peak amplitude analysis, positive peak and negative peak amplitudes are determined from the above filtered data. Further, the average of these peak amplitudes denotes  $A_p(f, r)$  or  $A_s(f, r)$  for P wave or S wave respectively. For coda wave however, the root mean square (RMS) amplitude of the filtered data denotes  $A_c(f, t_c)$ . On the other hand, in RMS amplitude analysis, all the values of  $A_p(f, r)$ ,  $A_s(f, r)$  and  $A_c(f, t_c)$  are denoted by the RMS amplitude of the filtered data of the respective waves. It has to be highlighted here that the peak amplitudes discussed above decay more quickly than RMS amplitude in case of direct waves. This results in a lesser attenuation value in RMS amplitude analysis in comparison to the peak amplitude analysis<sup>30</sup>. The above estimated values of  $A_p(f, r)$ ,  $A_s(f, r)$  and  $A_c(f, t_c)$  are further used to determine the values of  $\ln \left( \frac{A_s(f, r)r^\gamma}{A_c(f, t_c)} \right)$  and  $\ln \left( \frac{A_p(f, r)r^\gamma}{A_c(f, t_c)} \right)$ .

For the analysis, the value of  $\gamma$  equal to 1 is generally accepted as a good approximation for EQs with hypocentral depth greater than Moho discontinuity<sup>30</sup>. The above determined values of  $\ln \left( \frac{A_s(f, r)r^\gamma}{A_c(f, t_c)} \right)$  and  $\ln \left( \frac{A_p(f, r)r^\gamma}{A_c(f, t_c)} \right)$  are then plotted with the corresponding values of  $r$  over the ranges of  $f$ . Using the least square method, a linear fit can be found representing equation 5 and 8 for S and P wave respectively. The slope of above lines represents  $\frac{\pi f}{Q_s(f)v_s}$  and  $\frac{\pi f}{Q_p(f)v_p}$  respectively.

Once the value of slope is known, the values of  $Q_s$  and  $Q_p$  can be determined for known values of  $v_s$  and  $v_p$ . These

values of  $Q_s$  and  $Q_p$  are obtained for different ranges of  $f$ . Further, Fedotov and Boldyrev<sup>10</sup> assumed each value of  $Q$  to be a  $f$  dependent parameter expressed as:

$$Q = cf^n \quad (11)$$

Later, the coefficient  $c$  in the above equation was replaced by  $Q_o$  which represents the value of  $Q$  at 1Hz and  $n$  in equation (11) is the  $f$  dependent parameter defining the scale of medium heterogeneity<sup>16</sup>. Considering  $Q_o$ , the equation (11) was updated by Mak et al<sup>16</sup> as:

$$\log Q = n \log f + \log Q_o \quad (12)$$

Equation 12 again represents a straight line between  $\log Q$  and  $\log f$  with  $n$  being the slope and  $\log Q_o$  as the intercept. By values of  $Q$  obtained earlier, when plotted corresponding to their central frequencies ( $f_c$ ) on logarithmic scale (the range of  $f$  can be  $f_c \pm \frac{f_c}{3}$ ,  $f_c \pm \frac{f_c}{2}$  etc.), the values of  $Q_o$  and  $n$  can be determined. Further, the attenuation properties of the medium can be determined from the inverse of equation 10 as suggested below;

$$Q^{-1} = Q_o^{-1} f^{-n} \quad (13)$$

### Results

Aki<sup>3</sup> used CNM on more than 450EQ records at Tsukuba station in Japan and more than 400EQ records at Dodaira station in Japan to find out the  $Q_s$ . These EQ records were corresponding to magnitudes within the range of 3-4. The focal depths of above records were either close to 10km range or close to 70km range. Study area consisting of above two stations was divided into three regions A, B and C based on the tectonic activities. Region A covered all the epicentres where the EQs occurred due to the subduction of Pacific plate under the Eurasian plate, region B covered all the epicentres where EQs occurred due to the subduction of Philippine Sea plate and Pacific plate from the south as well as from the east. Region C consisted of all the epicentres where EQs occurred due to volcanic activities.

For the analyses, two regions [region A and region (B+C)] were considered separately considering six different values of  $f_c$  as 0.75, 1.5, 3.0, 6.0, 12.0 and 24.0Hz. A  $t_c$  of 50s from the origin was considered. A factor  $[P(\omega, t_c)/P(\omega, 50)]$  was multiplied to the coda wave data in case the data was obtained at  $t_c$  other than 50s where  $P(\omega, t_c)$  was the spectral density of coda wave at  $t_c$ . Above analyses results were shown separately for EQs with focal depth less than

35 km and beyond 35km. The obtained values of  $Q_S^{-1}$  were plotted against their corresponding  $f_c$  values as shown in figure 6 and 7. Both these figures show a decrease in  $Q_S^{-1}$  as  $f_c$  increases. From these attenuation plots (Figure 6 and 7), Aki<sup>3</sup> found the  $f$  dependent parameter  $n$  (equation 13) to be 0.8 for region A and 0.6 for regions (B+C).

Results obtained by Aki<sup>3</sup> were similar to  $n = 0.6$  for S waves in Kuril Islands found by Fedotov and Boldyrev<sup>10</sup> and  $n = 0.5$  for S waves at Garm in central Asia by Rautian and Khalturin<sup>20</sup>. In addition, obtained  $Q$  value for S wave by Aki<sup>3</sup> was found close to the  $Q$  value for coda wave by Rautian and Khalturin<sup>20</sup> indicating that coda waves are primarily composed of S waves. Aki<sup>3</sup> further proposed four possible reasons for S wave attenuation based on the observed  $f$  dependency of  $Q$  for S wave. These included:

- 1) Frictional dissipation of energy due to completely or partially filled cracks,
- 2) Adiabatic compression and dilation causing temperature variation and loss of kinetic energy,
- 3) Dislocation glide within the faults and
- 4) Loss of energy due to scattering.

Yoshimoto et al<sup>30</sup> extended CNM in order to determine the attenuation of direct P and S waves. EQs within  $r$  from 60 km to 160 km having the magnitude range of 2.1 – 5.5 and focal depth around 50km were considered. For the analyses a time window of 5s and  $t_c$  of 60s were considered by Yoshimoto et al<sup>30</sup>. Filtering of all the seismogram was done for five different ranges of  $f$  (1–2, 2–4, 4–8, 8–16 and 16–32Hz) using four pole Butterworth filter.

Further, Yoshimoto et al<sup>30</sup> performed the analysis using peak as well as RMS amplitude. Obtained results based on peak and RMS amplitude analyses by Yoshimoto et al<sup>30</sup> are represented in table 1 in the present work. It can be observed from table 1 that the peak amplitude decays faster than the RMS amplitude in case of both P as well as S wave. Another point which can be noticed from table 1 is that P wave attenuates faster than S wave for all the ranges of  $f$ . Thus, the ratio  $Q_P^{-1}/Q_S^{-1}$  becomes greater than unity. In addition, Yoshimoto et al<sup>30</sup> found the ratio  $Q_P^{-1}/Q_S^{-1}$  was equal to  $v_p/v_s$  which was found matching with Rautian et al.<sup>21</sup>

While extending the CNM, Yoshimoto et al<sup>30</sup> assumed the ratio  $s_s(f)/s_p(f)$  as same, within narrow ranges of  $f$  and EQs magnitude. To validate this assumption, Yoshimoto et al<sup>30</sup> determined the value of  $Q_p$  for EQs within the magnitude range of 2.5–3.5 and for EQs within the magnitude range of 2.1–5.5. Based on the analyses results, Yoshimoto et al<sup>30</sup> found no significant difference in the attenuation values obtained for both the above cases. This observation was convincing to hold the assumption on

$s_s(f)/s_p(f)$  to be same. For the above analyses, the value of  $\gamma$  was assumed to be 1. However, this value of  $\gamma$  may vary for crustal EQs where waves get reflected from the Conrad or Moho discontinuity<sup>30</sup>.

In order to validate this assumption, Yoshimoto et al<sup>30</sup> estimated the values of  $Q_p^{-1}$  and  $Q_s^{-1}$  for different values of  $\gamma$  (0.75, 1.00 and 1.50) and found no significant change. Although Yoshimoto et al<sup>30</sup> concluded that  $f$  dependence of attenuation becomes feeble with larger value of  $\gamma$ . Time window length is another important factor for this analysis and should be considered from the onset of the direct waves. In many cases, the peak amplitude of direct waves appears several seconds after the onset of direct wave. In such cases, a small time window may omit the peak amplitude part and can cause variation in the obtained value of attenuation.

Yoshimoto et al<sup>30</sup> used three different time window lengths of 3, 5 and 10s and found that the attenuation decreases slightly with increase in time window length. In addition, Yoshimoto et al<sup>30</sup> found that  $Q_s$  increases with focal depth.

Bennett and Bakun<sup>8</sup> studied the dependency of attenuation for EQs occurred at different depths within the lithosphere at Kanto area and concluded that  $f$  can be strongly correlated with  $Q_S^{-1}$  for EQs within the crust than the upper mantle. Bennett and Bakun<sup>8</sup> also reported that  $Q_S^{-1}$  increases with depth which was also confirmed by Yoshimoto et al<sup>30</sup>.

CNM has been used by many researchers (table 2) throughout the world to determine values of  $Q_p^{-1}$  and  $Q_s^{-1}$ . It can be observed from table 2 that CNM has been adopted to determine direct wave attenuation in significant parts of the globe. Further, based on the above obtained attenuation, the tectonic stability and wave propagation medium characteristics of each region were also attempted.

### Other methods for determination of $Q_p$ and $Q_s$ :

Apart from CNM, there are other methods too, developed by various researchers to determine the attenuation of waves in a region. Two such methods are discussed as below:

**Method 1:** Baruah et al<sup>7</sup> used the changes in spectral shapes of EQ to determine the direct wave attenuation at Jubilee Hills region at Hyderabad, India. These spectral shapes were obtained by First Fourier Transformation of acceleration time history. Spectral amplitude of direct wave  $A(f)$  can be represented by the following equation as:<sup>7</sup>

$$A(f) \propto \left[ \frac{A_o(f)R(f)e^{-\frac{\pi ft}{Q}}}{r} \right] \quad (14)$$

where  $A_o(f)$  represents the source spectral amplitude of direct wave,  $R(f)$  represents the site response function,  $t$  is the travel time of the corresponding direct wave. Logarithm of the ratio of  $A(f)$  at two different frequencies ( $f1$  and  $f2$ ) can be obtained as<sup>7</sup>:

$$\ln\left[\frac{A(f1)}{A(f2)}\right] = \ln\left[\frac{A_o(f1)}{A_o(f2)}\right] + \ln\left[\frac{R(f1)}{R(f2)}\right] - \left[\frac{\pi(f1-f2)t}{Q}\right] \quad (15)$$

In the above equation,  $\ln[A_o(f1)/A_o(f2)]$  and  $\ln[R(f1)/R(f2)]$  were assumed to be independent of  $t$ . The values of  $f1$  and  $f2$  were considered to be 8Hz and 28Hz and  $A(f)$  was found to vary between 6 to 10Hz and 26 to 30Hz respectively. Baruah et al<sup>7</sup> started the above analysis with the assumption that the value of  $A_o(f1)/A_o(f2)$  is same at 8 and 28 Hz for all the EQs. This assumption was validated later by plotting the values of  $A(f)$  at 8 and 28Hz with respect to  $r$  for EQs recorded at three temporary stations (PML, PSJ and AOU) of Jubilee Hills area, Hyderabad as shown in figure 8.

The values of  $A(f)$  shown in figure 8 can vary due to three factors i.e.  $A_o(f)$ , path propagation medium and site amplification factor. The effects due to the variation in propagation medium and site amplification factor in this case were not significant as all the records obtained at particular stations for EQs occurred in the nearby regions. Hence in this case, the only factor influencing the values of  $A(f)$  was  $A_o(f)$ .

Figure 8 shows that the decay of  $A(f)$  at 8 and 28Hz was similar at AOU station for all the EQ records. As a result,  $\ln[A_o(f1)/A_o(f2)]$  where,  $f1= 8\text{Hz}$  and  $f2= 28\text{Hz}$  was considered same for all EQs. The values of  $A(f1)$  and  $A(f2)$  were obtained from the Fast Fourier transformation. The values of  $\ln[A(f1)/A(f2)]$  were plotted against their corresponding values of  $t$ .  $Q$  for direct waves was then determined from the slope of regression line  $\pi(f1-f2)/Q$ . In the above study, an average value of  $Q$  over the entire  $f$  range was considered and obtained values of  $Q_p$  and  $Q_s$  by Baruah et al<sup>7</sup> were 0.0042 and 0.0036 respectively.

**Method 2:** Another method was proposed by Nakamura and Koyama<sup>17</sup> in order to determine the seismic  $Q$  of P and S waves in the upper mantle of Moon. It was a combination of single station method and multiple station method. The power spectral density  $P(\omega, T; s)$  for an event ( $s$ ) at a single station was represented as:<sup>17</sup>

$$P(\omega, T; s) = P_o(\omega; s)G(T) \exp\left[-\omega \int_0^T Q^{-1}(\omega, t) dt\right] \quad (16)$$

where  $P_o(\omega; s)$  was the power spectral density of  $s$  at the source,  $G(T)$  represents the geometrical spreading,  $\omega$  is the angular frequency and  $T$  as per Nakamura and Koyama<sup>17</sup> represents the travel time of seismic wave. For the analysis,  $G(T)$  was considered as  $T^{-n}$  where  $n=1$  for two dimensional geometric spreading and  $n=2$  for three dimensional geometric spreading. To find  $Q^{-1}(\omega)$ , double differentiation of natural logarithm of equation 16 was done first with respect to  $\omega$  and then with respect to  $T$ . Thus, the following differential equation was obtained<sup>17</sup>:

$$Q^{-1} + \omega \frac{dQ^{-1}}{d\omega} = F(\omega) \quad (17)$$

where  $F(\omega) = -\frac{d\left[\frac{\partial \ln P}{\partial \omega} + K_i\right]}{dt}$  and  $K_i$  is the station correction factor. The above differential equation (equation 17) was solved by Nakamura and Koyama<sup>17</sup> to obtain the following relation:

$$Q^{-1}(\omega) = \frac{1}{\omega} \int \omega F(\omega) d \ln \omega + \frac{C_o}{\omega} \quad (18)$$

where  $F(\omega)$  represents the slope of the regression line plotted between  $\partial \ln P / \partial \omega$  and  $t$  as presented in figure 9. It has to be highlighted here that figure 9 only shows the plot between  $\partial \ln P / \partial \omega$  and  $t$  for P wave within the range of 4.1-6.2Hz. The slope of the regression line in figure 9 gave the value of  $F(\omega)$ . However, for other ranges of  $f$ ,  $F(\omega)$  obtained for P and S wave by Nakamura and Koyama<sup>17</sup> are shown in figures 10 and 11 respectively. Obtained values of  $F(\omega)$  above were used to find the first term in the equation 18. In order to find out the constant ( $C_o$ ) in the second term of equation 18, multiple station methods were used based on the following expression for determining attenuation by Nakamura and Koyama:<sup>17</sup>

$$Q^{-1}(\omega) = \frac{d[-\ln P(\omega) + \ln G(T) - \ln L_i(\omega)]}{\omega dT} \quad (19)$$

where  $L_i(\omega)$  represented the local station correction as the spectral content varies at each station due to the differences in the local geology at that station<sup>17</sup>. Later,  $Q^{-1}$  was obtained from the slope of the linear regression line from the plots between  $\ln P$  and  $\omega T$ .  $G(T)$  in equation 19 was replaced by  $T^{-n}$  and  $n$  values were considered between 1 and 2. The values of  $L_i$  for all the stations were determined from the regression analysis. The constant  $C_o$  was estimated using the least square method by minimizing the difference between results obtained from single and multiple station method.

Obtained value of  $C_o$  was substituted back in the equation 18 to determine the final value of  $Q^{-1}$ . Obtained values of  $Q_p^{-1}$  and  $Q_s^{-1}$  by Nakamura and Koyama<sup>17</sup> are enumerated in

table 3. Values of  $Q_p^{-1}$  and  $Q_s^{-1}$  from table 3 reflect a low rate of attenuation in moon's interior than earth's interior.  $Q_p^{-1}$  was found to be increasing with the increasing  $f$ , however in case of  $Q_s^{-1}$ , opposite trend was observed.

**Discussion**

P and S waves are compressional and shear wave respectively. Both these waves attenuate differently. As discussed earlier, in table 2 the summary of direct P and S wave attenuation for various regions across the globe including India, Japan, Korea, Iran, Italy etc. is presented. It can be seen from table 2 that P wave attenuates faster than S wave. This indicates that  $Q_p^{-1}/Q_s^{-1}$  is greater than 1. As per Parvez et al<sup>19</sup>,  $Q_p^{-1}/Q_s^{-1}$  greater than 1 implicates large volume of dry rocks as a propagation medium throughout these regions. As S wave cannot pass through fluids<sup>19</sup>, it attenuates faster in case of saturated or weathered rocks and thus  $Q_p^{-1}/Q_s^{-1}$  becomes less than 1. The values of  $Q_p^{-1}$  and  $Q_s^{-1}$  also demarcate the tectonic activity of any region.

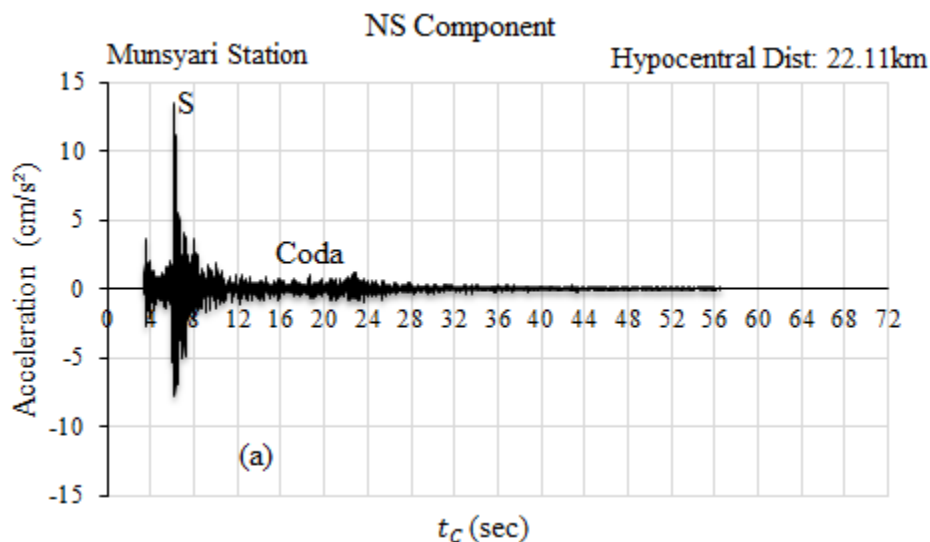
**Tectonic Activity:** Japan which is tectonically very active region shows a high value for both  $Q_p^{-1}$  and  $Q_s^{-1}$  compared to the region of South Korea as can be seen from table 2. In addition, table 2 also shows higher values of  $Q_p^{-1}$  and  $Q_s^{-1}$  in the Himalayan region which is tectonically one of the most active regions of the globe. It has to be highlighted here that tectonically active region here indicates those regions which are either near to the plate boundaries or in case an active EQ source exists near to the region. The presence of faults, folds, dykes or sills makes the medium

heterogeneous and eventually causing more attenuation of seismic waves in the region.

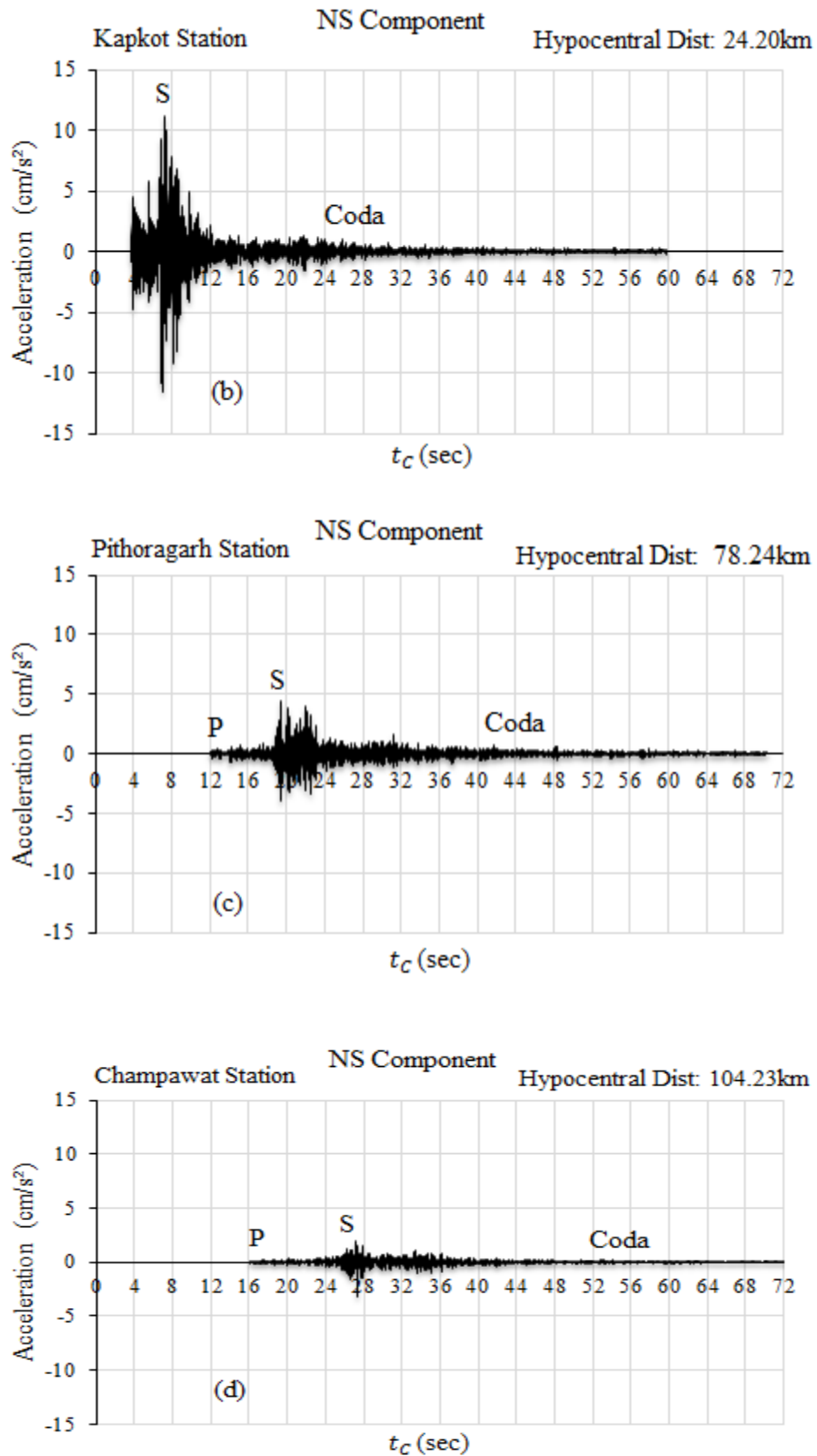
Nakamura and Koyama<sup>17</sup> showed the values of  $Q_p^{-1}$  and  $Q_s^{-1}$  for moon's interior as very less comparative to any region on the earth. The reason behind this is that the moon is pretty smaller in size in comparison to the earth. Hence, there is no convection current present inside the moon to cause any tectonic activity which can cause high attenuation of seismic waves as happens in case of the earth<sup>26</sup>. The values of  $Q_p^{-1}$  and  $Q_s^{-1}$  used above can be determined from any of the three methods discussed earlier.

**Assumptions among different methods:** In the present work, the methodology for CNM is discussed elaborately. In order to compare the values of  $Q_p^{-1}$  and  $Q_s^{-1}$  obtained by CNM and other methods, two additional methods are also discussed. However, each of these three methods has their own assumptions. In all the methods,  $Q$  was assumed to be varying with  $f$ . In CNM and the third method,  $Q$  was expressed in terms of  $f$  whereas in second method, an average value of  $Q$  was obtained for the entire  $f$  range. In CNM, to obtain the value of  $Q_p^{-1}, s_s(f)/s_p(f)$  was assumed same for a narrow range of  $f$ . In the second method,  $\ln[A_o(f1)/A_o(f2)]$  and  $\ln[R(f1)/R(f2)]$  were assumed as variables of  $f$  but independent of  $t$ .

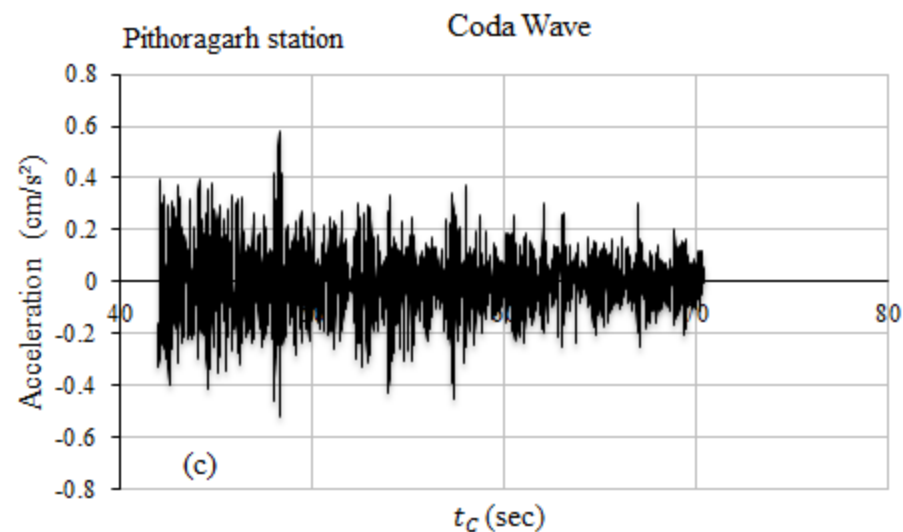
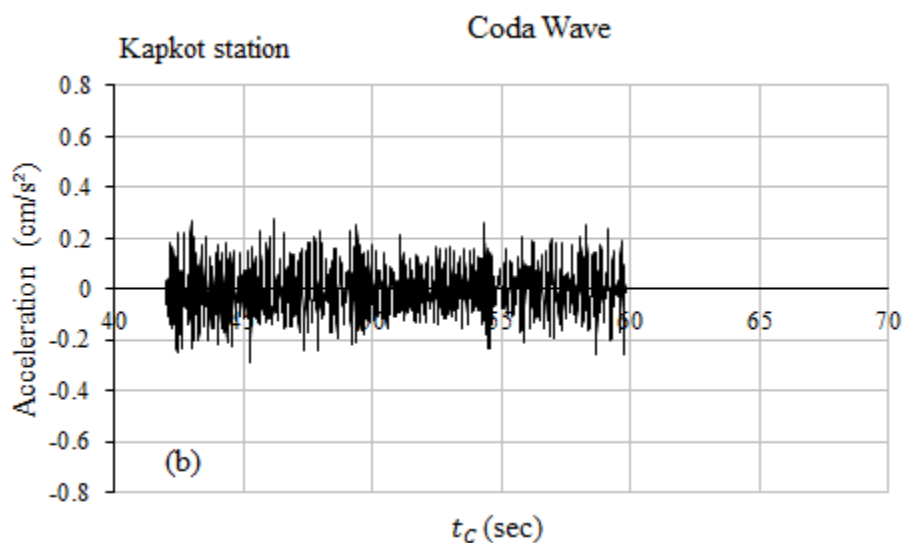
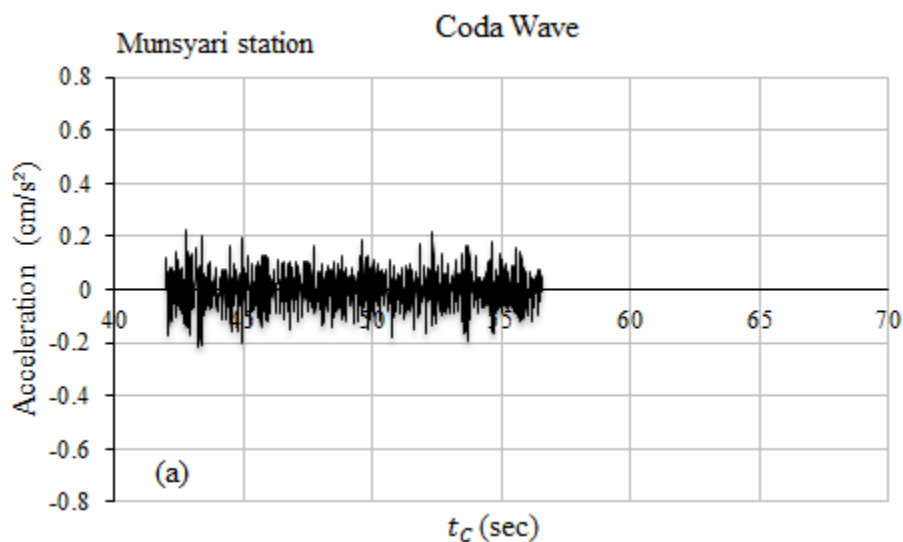
Thus, all these assumptions suggest that  $f$  is a very important parameter in defining the attenuation of a medium.







**Figure 1: August 2008 EQ (Latitude: 30.1 N, Longitude: 80.1 E) recorded at 4 stations (Munsyari, Lat.: 30.066 N, Long.: 80.237 E; Kapkot, Lat.: 29.941 N, Long.: 79.899 E; Pithoragarh, Lat.: 29.579 N, Long.: 80.207 E; Champawat, Lat.: 29.334 N, Long.: 80.095 E) illustrating the attenuation of seismic waves**



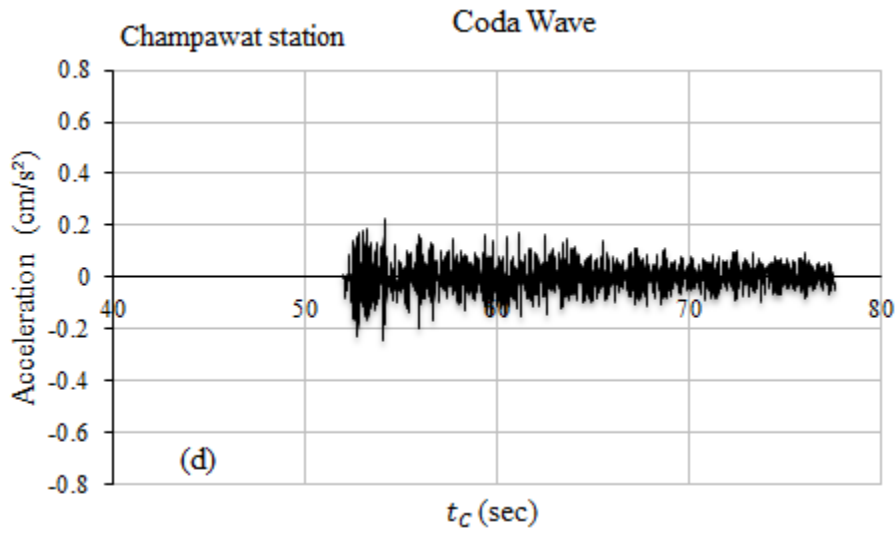


Figure 2: Enlarged coda wave portion from corresponding figure 1

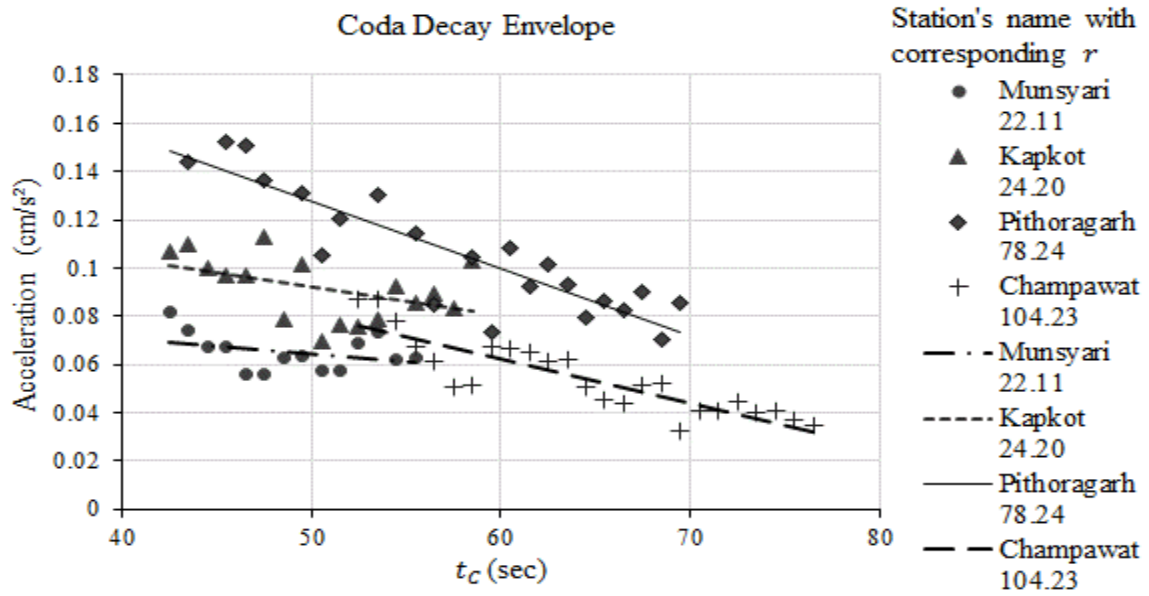
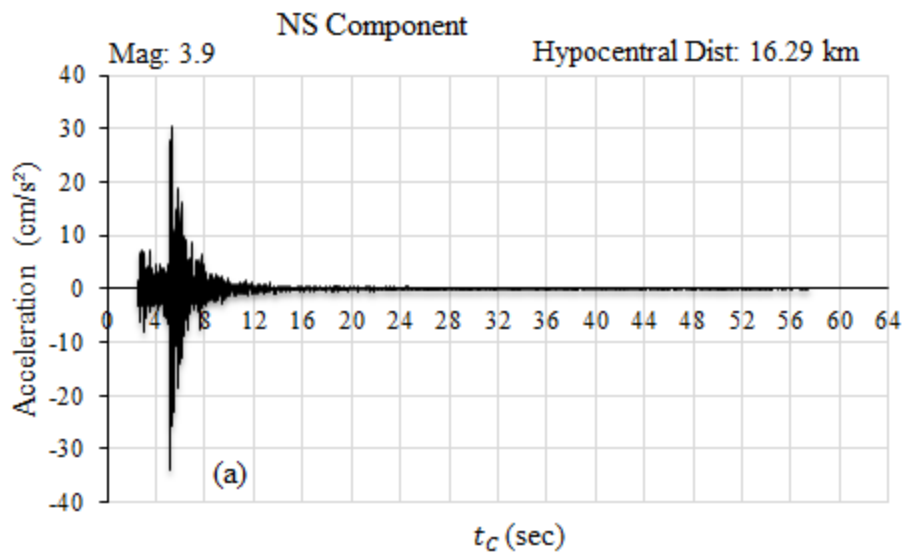
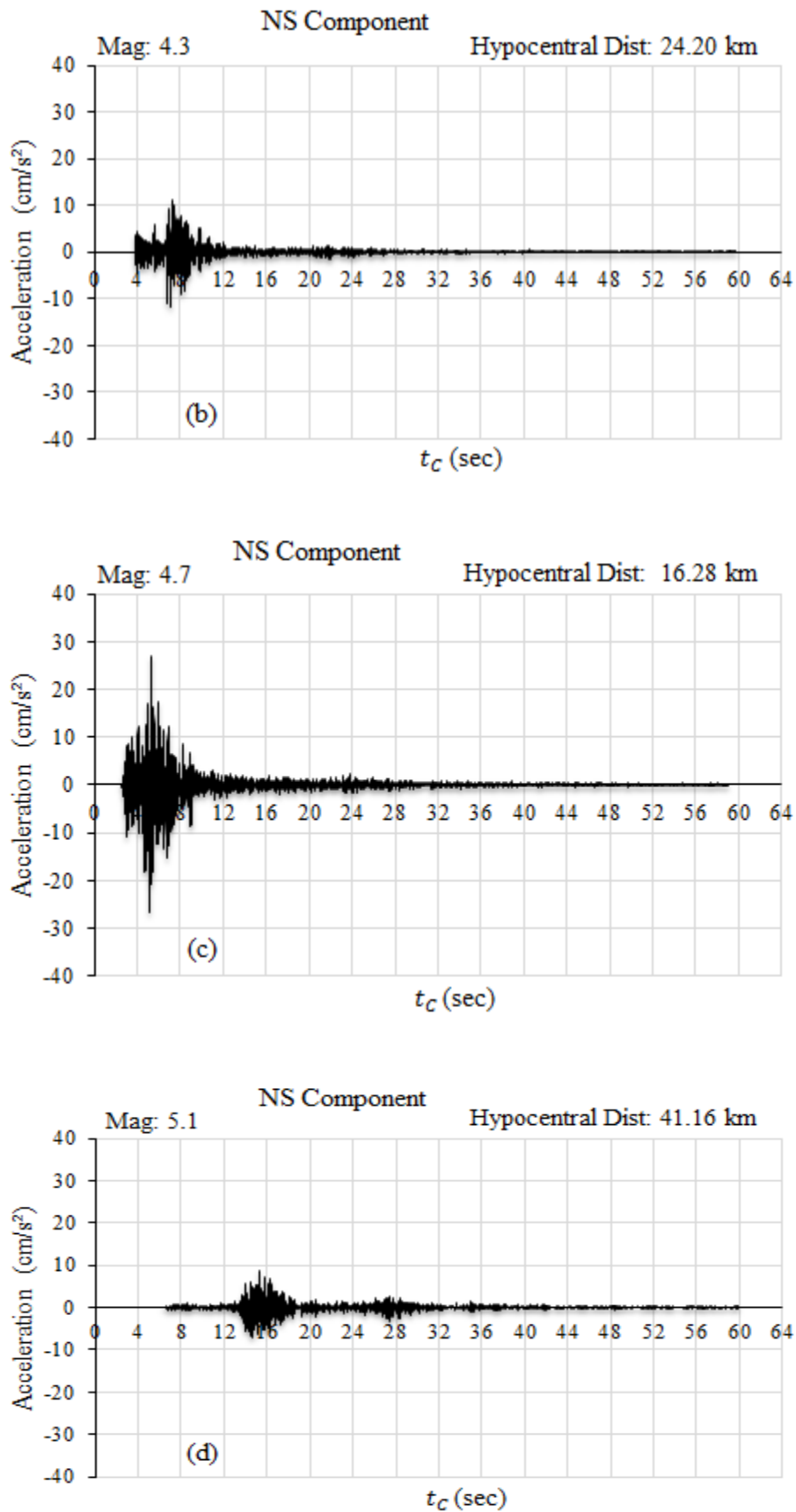


Figure 3: Coda decay envelope at four stations for the records shown in figure 2





**Figure 4: Records of 4 EQs (Aug'2009, Lat.:30.0 N Long.: 80.0 E; Aug'2008, Lat.: 30.1 N Long.: 80.1 E; Feb'2010, Lat.: 30.0 N Long.: 80.1 E; Sep'2008, Lat.: 30.1 N Long.: 80.4 E) recorded at Kapkot station (Lat.: 29.941 N, Long.: 79.899 E)**

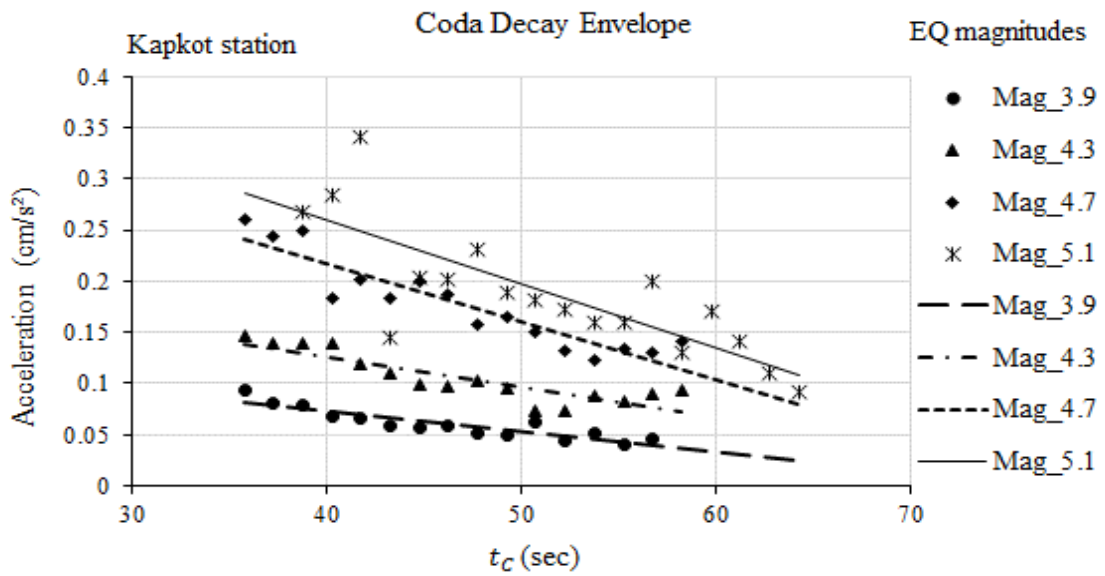


Figure 5: Coda decay envelope at Kapkot station for EQ records shown in figure 4

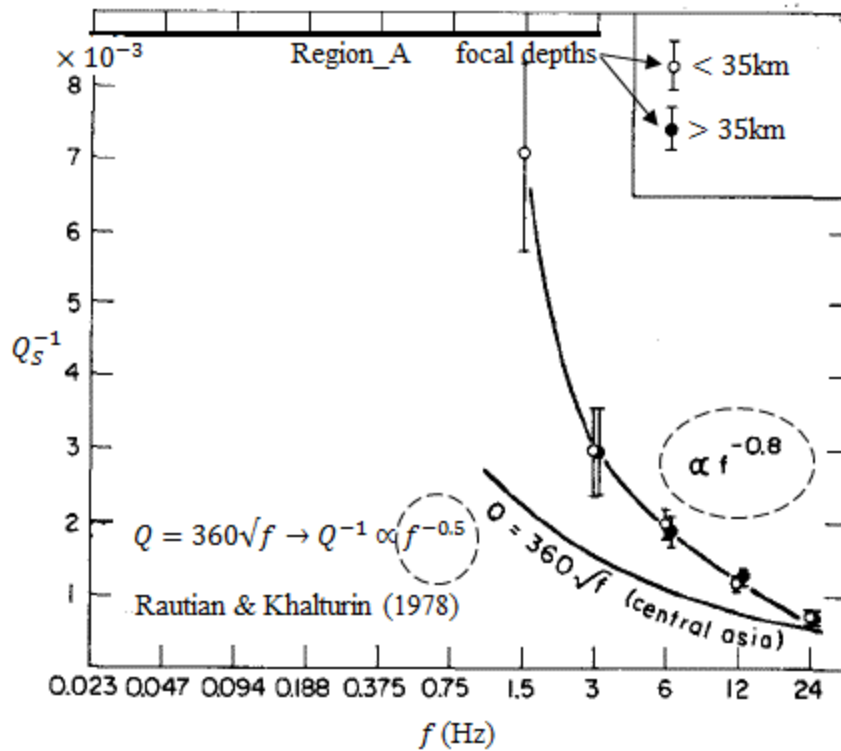


Figure 6: The frequency dependent attenuation of S wave for region A is shown in the enclosed portion. The frequency dependent relation for central Asia<sup>20</sup> is also shown for comparison [Modified after Aki<sup>3</sup>]

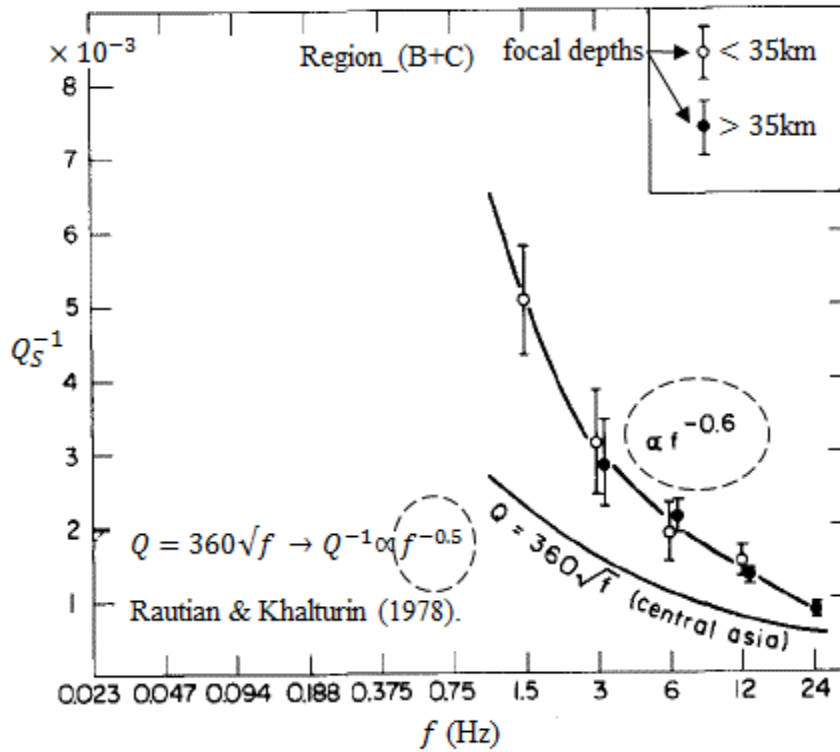


Figure 7: The frequency dependent attenuation of S wave for region B+C is shown in the enclosed portion. The frequency dependent relation for central Asia<sup>20</sup> is also shown for comparison [Modified after Aki<sup>3</sup>]

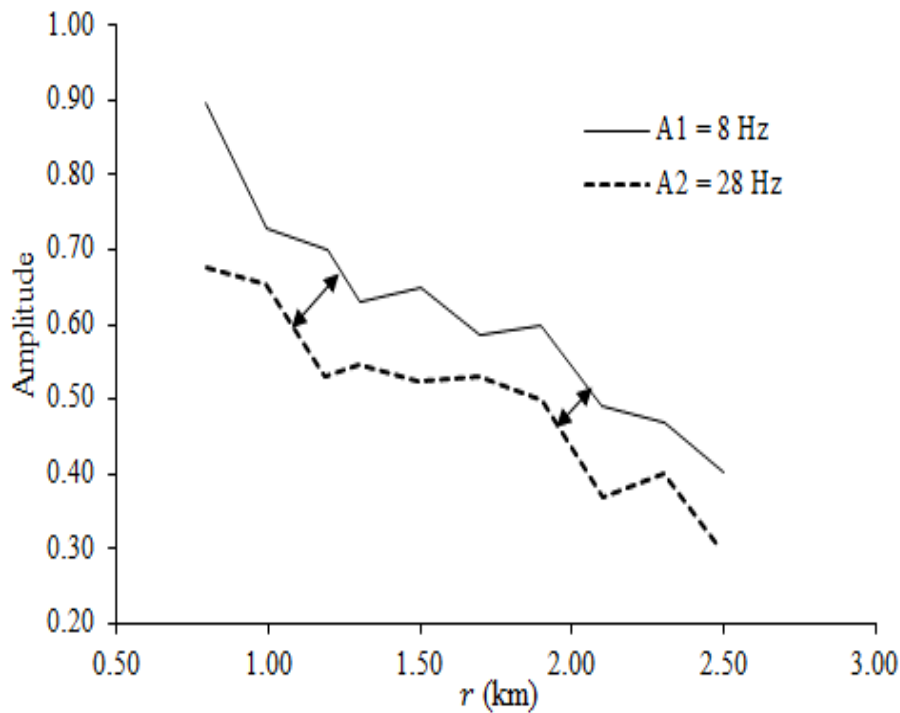


Figure 8: Decay of spectral amplitude at 8 and 28 Hz with respect to  $r$  for different earthquakes at a single station [Modified after Baruah et al<sup>7</sup>]

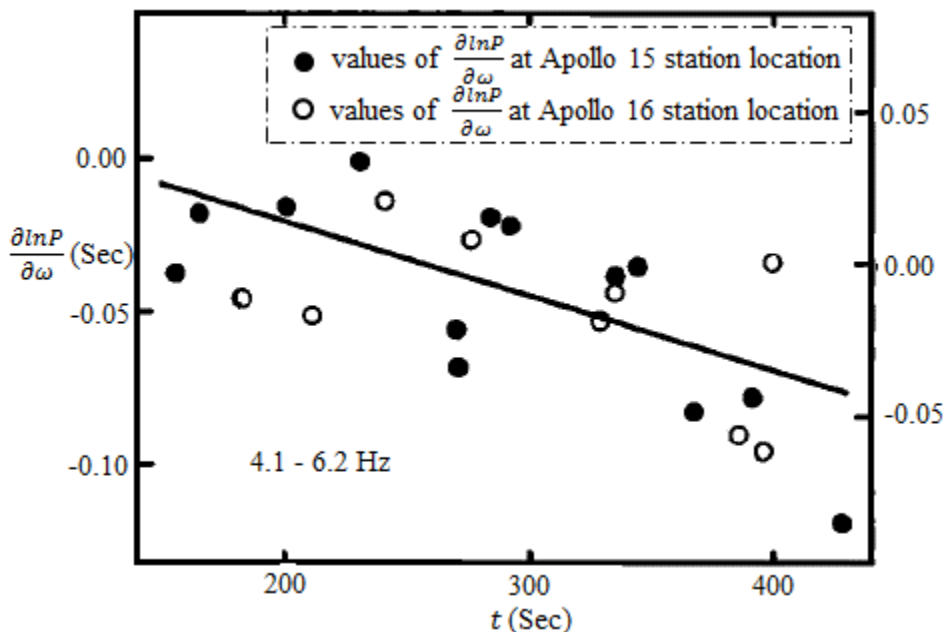


Figure 9: The regression line from the plot of  $\frac{\partial \ln P}{\partial \omega}$  against their corresponding  $t$  for P wave for a single moonquake recorded at Apollo 15 station (black dots) and Apollo 16 station (white dots). The values of  $\frac{\partial \ln P}{\partial \omega}$  were plotted according to the left hand side scale for Apollo 15 site and according to right hand side scale for Apollo 16 site due to differences in local geological structures as per Nakamura and Koyama<sup>17</sup>.  
 [Modified after Nakamura and Koyama<sup>17</sup>]

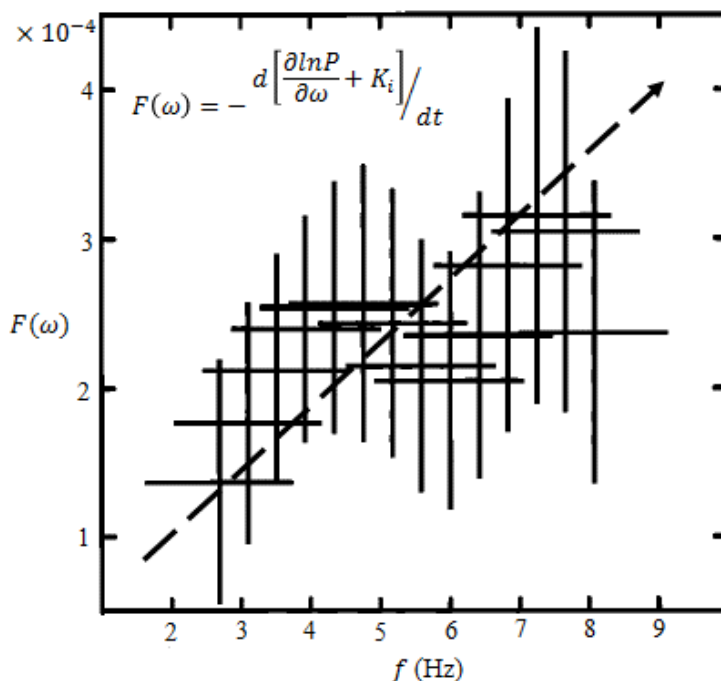


Figure 10: Plot of  $F(\omega)$  values against their corresponding  $f$  (Hz) for P wave. The arrow shown in dotted line demarcates the increasing trend of  $F(\omega)$  values with  $f$ . The Horizontal line represents the  $F(\omega)$  value for the entire frequency band and the vertical line represents the corresponding standard errors.  
 [Modified after Nakamura and Koyama<sup>17</sup>]

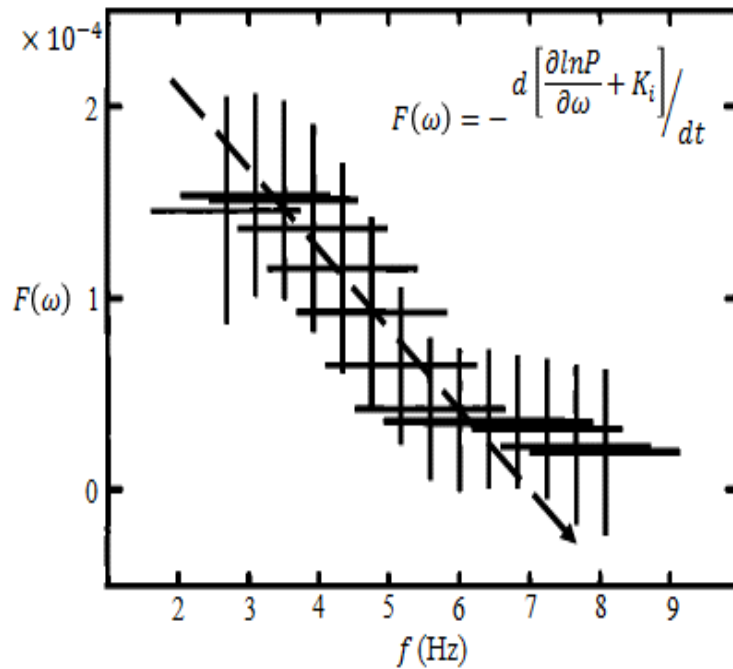


Figure 11: Plot of  $F(\omega)$  values against their corresponding  $f$  (Hz) for S wave. The arrow shown in dotted line demarcates the decreasing trend of  $F(\omega)$  values with  $f$ . The Horizontal line represents the  $F(\omega)$  value for the entire frequency band and the vertical line represents the corresponding standard errors. [Modified after Nakamura and Koyama<sup>17</sup>]

Table 1  
Attenuation of P and S wave obtained from peak and RMS amplitude analysis<sup>30</sup>

Wave type	Peak amplitude analysis	RMS amplitude analysis
P wave	$Q_P^{-1} = 0.031 f^{-0.95}$	$Q_P^{-1} = 0.026 f^{-0.95}$
S wave	$Q_S^{-1} = 0.012 f^{-0.73}$	$Q_S^{-1} = 0.009 f^{-0.68}$

Table 2  
Attenuation of P and S wave obtain worldwide using CNM

Researchers	Place	$Q_P^{-1}$	$Q_S^{-1}$
Yoshimoto et al <sup>30</sup>	Western Nagano, Japan	$0.052 f^{-0.66}$	$0.0034 f^{-0.12}$
Chung and Sato <sup>9</sup>	SE South Korea	$(0.009 \pm 0.003) f^{(-1.05 \pm 0.14)}$	$(0.004 \pm 0.001) f^{(-0.70 \pm 0.14)}$
Tuve et al <sup>29</sup>	Straits of Messina, Southern Italy	-----	$0.016 f^{-0.70}$
Zareanet al <sup>32</sup>	Qeshm Island, Iran	$0.1 f^{-0.83}$	$0.06 f^{-0.97}$
Sharma et al <sup>24</sup>	Chamoli Region, India	$(0.023 \pm 0.0005) f^{(-0.82 \pm 0.04)}$	$(0.0115 \pm 0.0004) f^{(-0.71 \pm 0.03)}$
Ma'hood et al <sup>15</sup>	East Central Iran	$(0.025 \pm 0.003) f^{(-0.99 \pm 0.04)}$	$(0.019 \pm 0.002) f^{(-1.02 \pm 0.06)}$
Ali K. <sup>1</sup>	Cairo (Egypt)	$(0.019 \pm 0.002) f^{(-0.8 \pm 0.1)}$	$(0.007 \pm 0.001) f^{(-0.85 \pm 0.1)}$
Padhay and Subhadra <sup>18</sup>	North-East India	$(0.035 \pm 0.014) f^{(-0.96 \pm 0.01)}$	$(0.014 \pm 0.006) f^{(-0.94 \pm 0.03)}$
Singh et al <sup>25</sup>	Kumaun Himalaya (India)	$(0.045 \pm 0.009) f^{(-1.35 \pm 0.04)}$	$(0.0096 \pm 0.0009) f^{(-1.3 \pm 0.03)}$
Parvez et al <sup>19</sup>	North-Western Himalaya	$(0.0103 \pm 0.0003) f^{(-1.06 \pm 0.06)}$	$(0.0078 \pm 0.0003) f^{(-0.96 \pm 0.06)}$
Tripathi et al <sup>27</sup>	Garhwal Himalaya (India)	$(0.027 \pm 0.003) f^{(-1.16 \pm 0.06)}$	$(0.008 \pm 0.0007) f^{(-0.93 \pm 0.05)}$
Sharma et al <sup>23</sup>	Delhi (India)	$(0.019 \pm 0.001) f^{(-1.03 \pm 0.07)}$	$(0.0102 \pm 0.0007) f^{(-1.07 \pm 0.09)}$
Banerjee and Kumar <sup>6</sup>	Chamba region, India	$0.0102 f^{-0.96}$	$0.0058 f^{-0.87}$



**Table 3**  
**Attenuation of P and S wave at 3 and 8 Hz frequency in lunar upper mantle<sup>30</sup>**

Wave Attenuation	3 Hz	8 Hz
$Q_p^{-1}$	< 0.00025	0.00025 - 0.000125
$Q_s^{-1}$	0.00025 - 0.000067	0.000143 - 0.000067

Additionally in CNM, average  $v_p$  and  $v_s$  values are assumed for the analysis which requires a velocity model to be known for the region. These velocities ( $v_p$  and  $v_s$ ) are considered constant throughout the entire seismic wave propagation path whereas in reality there can be variation in velocities due to the changes in the medium characteristics. This may cause further attenuation of seismic waves.

### Conclusion

During an EQ event, various kinds of waves are recorded at a seismic recording station. These include direct waves as well as backscattered waves. Between the EQ source and the recording station, a gradual decay in the wave amplitude happens which is known as attenuation of seismic waves. A seismic wave gets attenuated due to three possible reasons namely geometric spreading, scattering of seismic energy and inelasticity of the propagation medium. Coda waves which are backscattered waves generate due to medium heterogeneity and arrive at the tail end of the seismogram. The amplitude of coda wave is independent of  $r$  as well as magnitude.

Normalization of direct wave with respect to the coda was utilized while developing the CNM in order to determine the P and S wave attenuation in a region. Details about CNM and the procedure to be followed are discussed in this paper. In addition, detailed review on other two methods developed to assess the attenuation of direct wave is also presented. A brief discussion regarding the assumptions made by each of the methods, validation and the obtained attenuation values is presented. These values of attenuation can infer information about the tectonic stability, medium heterogeneity etc. of a region. Correlating the values of  $Q_p^{-1}$  and  $Q_s^{-1}$ , rock types in a region can also be determined.

Using the single backscattering model, attenuation of coda wave and its comparison with the direct wave attenuation values in order to obtain the scale of scattering within the medium can be attempted in the future. In general, the attenuation values obtained from the above methods are combinations of various attenuation types. Methods which can determine the intrinsic and scattering attenuations separately from the direct wave attenuation values are not covered in the present review work but can be attempted in the future in order to obtain a detailed characterization of the wave propagation medium.

### References

1. Ali Abdel-Fattah K., Attenuation of body waves in the crust beneath the vicinity of Cairo Metropolitan Area (Egypt) using coda normalization method, *Geophys J Int.*, **176**, 126-134 (2009)
2. Aki K., Analysis of the Seismic Coda of Local Earthquakes as Scattered Waves, *J Geophys Res*, **74(2)**, 615-631 (1969)
3. Aki K., Attenuation of Shear-Waves in the Lithosphere for Frequencies from 0.05 to 25 Hz, *Phys Earth Planet*, **21**, 50-60 (1980)
4. Aki K. and Chouet B., Origin of Coda Waves: Source, Attenuation, and Scattering Effects, *J Geophys Res*, **80(23)**, 3322-3342 (1975)
5. Anbazhagan P., Kumar Abhishek and Sitharam T.G., Ground Motion Predictive Equation Based on recorded and Simulated Ground Motion Database, *Soil Dynam Earthquake Eng*, **53**, 92-108 (2013)
6. Banerjee S. and Kumar A., Attenuation of P and S wave for Chamba Region, Proc 50th Indian Geotechnical Conference, COEP, Pune, 17-19 (2015)
7. Baruah S., Hazarika D., Gogoi N.K. and Raju P.S., The effects of attenuation and site on the spectra of microearthquakes in the Jubilee Hills region of Hyderabad, India, *J Earth Syst Sci.*, **116(1)**, 37-47 (2007)
8. Bennett H.F. and Bakun W.H., Comment on attenuation of shear waves in the lithosphere for frequencies from 0.05 to 25 Hz, *Phys Earth Planet*, **29**, 195-196 (1982)
9. Chung T.W. and Sato H., Attenuation of High Frequency P and S waves in the crust of Southeastern South Korea, *Bull Seismol Soc Am*, **91(6)**, 1867-1874 (2001)
10. Fedotov S.A. and Boldyrev S.A., Frequency dependence of the body wave absorption in the crust and the upper mantle of the Kuril-Island chain, *Izv Akad Nauk USSR Earth Phys*, **9**, 17-33 (1969)
11. Sato H., Fehler M.C. and Maeda T., Phenomenological Study of Coda Waves, Seismic Wave Propagation and Scattering in the Heterogeneous Earth, 2nd ed., Springer, Verlag Berlin Heidelberg, 63-123 (2012)
12. Jeffrey G., Geophysics 224 Seismic 1, Geophysical & Environmental Sciences, University of Alberta Web, <https://www.ualberta.ca/~ygu/courses/geoph224/notes.html> accessed November 2015 (2014)
13. Knopoff L., *Q. Rev Geophys*, **2(4)**, 625-660 (1964)

14. Kumar N., Parvez I.A. and Virk H.S., Estimation of coda wave attenuation for NW Himalayan region using local earthquakes, *Phys Earth Planet*, **151**, 243-258 (2005)
15. Ma'hood M., Hamzehloo H. and Doloei G.J., Attenuation of High frequency P and S waves in the crust of East-Central Iran, *Geophys J Int.*, **179**, 1669-1678 (2009)
16. Mak S., Chan L.S., Chandler A.M. and Koo R.C.H., Coda Q estimates in the Hong Kong region, *J Asian Earth Sci.*, **24**, 127-136(2004)
17. Nakamura Y. and Koyama J., Seismic Q of the Lunar Upper Mantle, *J Geophys Res*, **87(B6)**, 4855-4861(1982)
18. Padhy S. and Subhadra N., Frequency dependent attenuation of P and S waves in northeast India, *Geophys J Int.*, **183**, 1052-1060 (2010)
19. Parvez I.A., Yadav P. and Nagaraj K., Attenuation of P, S and Coda Waves in the NW-Himalayas, India, *Int J Geosci*, **3**, 179-191 (2012)
20. Rautian T.G. and Khalturin V.I., The use of coda for determination of the earthquake source spectrum, *Bull Seismol Soc Am*, **68**, 923-948 (1978)
21. Rautian T.G., Khalturin V.I., Martynov V.G. and Molnar P., Preliminary analysis of the spectral content of P and S waves from local earthquakes in the Garm, Tadjiikatan region, *Bull Seismol Soc Am*, **68**, 949-971(1978)
22. Scheimer J. and Landers T.E., Short-period coda of a local event at Lassa, Seismic Discrimination, Semi-annual Technical Summary 42, Lincoln Lab, Massachusetts Institute of Technology, Cambridge (1974)
23. Sharma B., Chingtham P., Sutar A.K., Chopra S. and Shukla H., Frequency dependent attenuation of seismic waves for Delhi and surrounding area India, *Ann Geophys*, **58(2)**, S0216, doi:10.4401/ag-6636(2015)
24. Sharma B., Teotia S.S., Kumar D. and Raju P.S., Attenuation of P and S waves in the Chamoli Region, Himalaya, India, *Pure Appl Geophys*, **166**, 1949-1966 (2009)
25. Singh C., Singh A., Bharathi V.K.S., Bansal A.R. and Chadha R.K., Frequency dependent body wave attenuation characteristics in the Kumaun Himalaya, *Tectonophysics*, **524-525**, 37-42, doi:10.1016/j.tecto.2011.12.2013 (2012)
26. Tectonism, Lunar and Planetary Institute web, [http://www.lpi.usra.edu/education/explore/shaping\\_the\\_planets/tectonism.shtml](http://www.lpi.usra.edu/education/explore/shaping_the_planets/tectonism.shtml), Accessed 19th Feb, 2016 (2015)
27. Tripathi J.N., Singh P. and Sharma M.L., Attenuation of high-frequency P and S waves in Garhwal Himalaya, India, *Tectonophysics*, **636**, 216-227 (2014)
28. Tsujiura M., Spectral Analysis of the Coda Waves from Local Earthquakes, *Bulletin of the Earthquake Research Institute*, **53**, 1-48 (1978)
29. Tuve T., Bianco F., Ibanez J., Patane D., Del Pezzo E. and Bottari A., Attenuation study in the straits of Messina area (Southern Italy), *Tectonophysics*, **421**, 173-185 (2006)
30. Yoshimoto K., Sato H. and Ohtake M., Frequency-dependent attenuation of P and S waves in the Kanto area, Japan, based on the coda-normalization method, *Geophys J Int.*, **114**, 165-174(1993)
31. Yoshimoto K., Sato H., Yoshihisa I., Ito H., Ohminato T. and Ohtake M., Frequency-dependent attenuation of high frequency P and S waves in the upper crust in Western Nagano, Japan, *Pure Appl Geophys*, **153**, 489-502 (1998)
32. Zarean A., Farrokhi M. and Chaychizadeh S., Attenuation of high frequency P and S waves in Qeshm Island, Iran, Proceedings of 14th world conference on earthquake engineering, Oct 12-17, Beijing, China(2008).

(Received 20<sup>th</sup> April 2016, accepted 13<sup>th</sup> May 2016)

\*\*\*\*\*